

Article

The Design Strategy for an Aggregation- and Crystallization-Induced Emission-Active Molecule Based on the Introduction of Skeletal Distortion by Boron Complexation with a Tridentate Ligand

Shunsuke Ohtani , Masayuki Gon, Kazuo Tanaka *  and Yoshiki Chujo

Department of Polymer Chemistry, Graduate School of Engineering, Kyoto University, Katsura, Nishikyo-ku, Kyoto 615-8510, Japan; ohtani@poly.synchem.kyoto-u.ac.jp (S.O.); gon@poly.synchem.kyoto-u.ac.jp (M.G.); chujo@poly.synchem.kyoto-u.ac.jp (Y.C.)

* Correspondence: tanaka@poly.synchem.kyoto-u.ac.jp

Received: 25 June 2020; Accepted: 13 July 2020; Published: 15 July 2020



Abstract: We describe here a new design strategy for obtaining boron complexes with aggregation- and crystallization-induced emission (AIE and CIE, respectively) properties based on the introduction of skeletal distortion. According to our recent results, despite the fact that an almost planar structure and robust conjugation were obtained, the boron azomethine complex provided a slight emission in solution and an enhanced emission in aggregation and crystal. Quantum calculation results propose that unexpected emission annihilation in solution could be caused through intramolecular bending in the excited state. Herein, to realize this unique molecular motion and obtain AIE and CIE molecules, the phenyl quinoline-based boron complexes **BPhQ** and **BPhQm** with distorted and planar structures were designed and synthesized, respectively. **BPhQm** showed emission in solution and aggregation-caused quenching (ACQ, **BPhQm**: $\Phi_{F,sol.} = 0.21$, $\Phi_{F,agg.} = 0.072$, $\Phi_{F,cryst.} = 0.051$), while **BPhQ** exhibited a typical AIE and CIE (**BPhQ**: $\Phi_{F,sol.} = 0.008$, $\Phi_{F,agg.} = 0.014$, $\Phi_{F,cryst.} = 0.017$). The optical data suggest that a large degree of molecular motion should occur in **BPhQ** after photo-excitation because of the intrinsic skeletal distortion. Furthermore, single-crystal X-ray diffraction data indicate that the distorted π -conjugated system plays a positive role in presenting solid-state emission by inhibiting consecutive π - π interactions. We demonstrate in this paper that the introduction of the distorted structure by boron complexation should be a new strategy for realizing AIE and CIE properties.

Keywords: quinoline; boron complex; solid-state emission; aggregation-induced emission

1. Introduction

Organic fluorescent dyes have attracted considerable attention as a platform for constructing fluorescent probes to monitor biological events because of their various advantages, such as high sensitivity, rapid response, and property tenability [1–3]. In addition, organic fluorescent dyes can also be utilized for modern electronic devices, such as organic light-emitting diodes [4–6] and lighting panels [7]. Therefore, the development of a new type of fluorescent organic dye is a topic of interest in organic chemistry as well as material science. Recently, we proposed the concept of “element-blocks”, which are minimum functional units containing heteroatoms, to create functional materials according to preprogrammed designs [8–10]. In the series of studies on organic luminescent dyes containing heteroatoms, unique optical properties originating from heteroatoms have been revealed [11]. In particular, boron-containing element-blocks are promising building blocks for obtaining luminescent materials. Boron-fused structures with bidentate π -conjugated ligands can

enhance the rigidity and planarity of molecular frameworks because of their strong coordination ability originating from the electron-acceptor character of boron [12–16]. Thus, boron complexation is recognized as an established tactic for constructing highly-emissive fluorescent dyes [17–24]. Indeed, numerous studies have been accomplished on the development of emissive materials based on boron complexes with rigid and planar skeletons [25–30]. However, in solid states, planar organic chromophores often show the consecutive π – π stacking and subsequent physical interactions (e.g., energy transfer, inter- or intramolecular charge transfer, and excited states reactions). As a result, emission annihilation, called aggregation-caused quenching (ACQ), inevitably occurs [31,32]. Thus, most organic luminescent materials suffer from ACQ, especially in applications in luminescent devices.

As one of the critical solutions for overcoming ACQ, aggregation-induced emission (AIE) properties [33,34] and crystallization-induced emission (CIE) properties [35–37] have attracted attention. The AIE- and CIE-active molecules show enhanced emission by aggregation and crystallization, respectively. In dilute solutions, crucial intramolecular motions such as rotation and vibration occur, and their excited states are readily decayed through non-radiative pathways. These motions would be restricted in solid form, followed by significant luminescence. Furthermore, by modulating the degree of molecular motions in the excited state, environment-responsive behaviors are often observed [38,39]. Therefore, the deep understanding of molecular motions in the excited state and the relationship with these motions and photochemical processes is necessary for designing advanced AIE and CIE-active dyes.

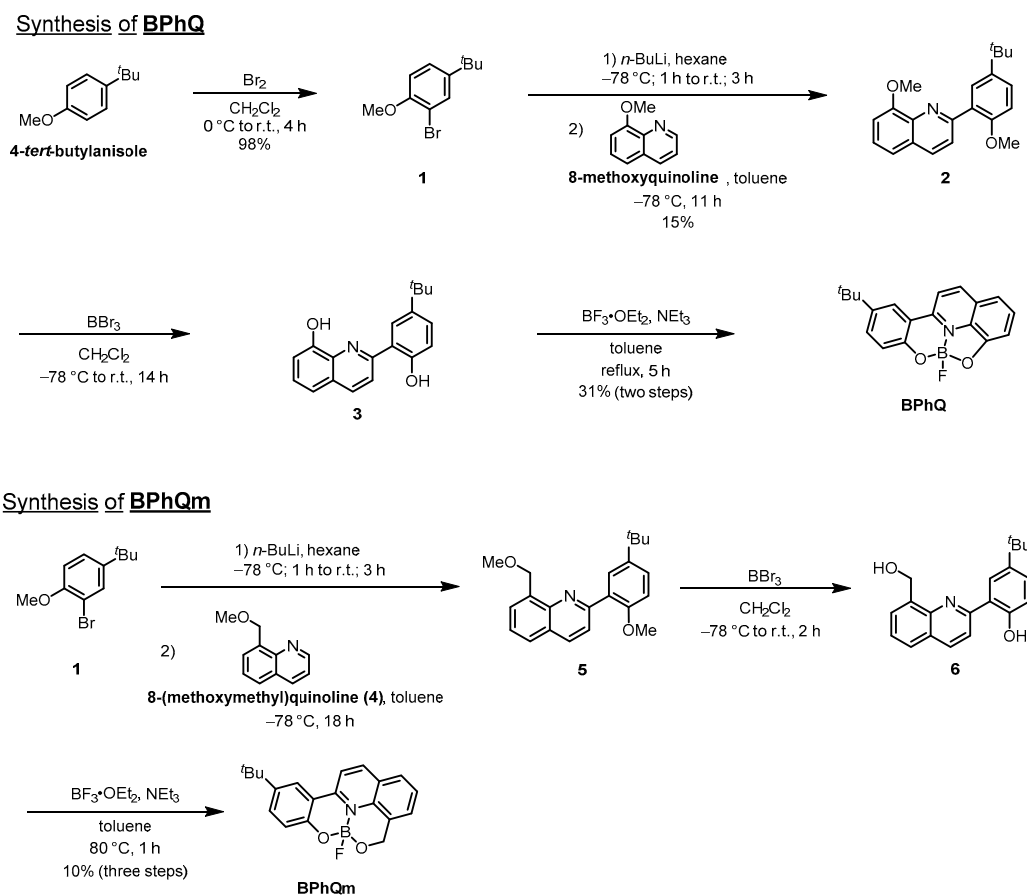
In our previous work, we synthesized a fused azomethine–boron complex with a slightly-distorted π -conjugated system and a protruded substituent on the boron atom [40]. Although these structural features are favorable for obtaining solid-state emission by disturbing nonspecific π – π interactions in the condensed state, the boron azomethine complex is an AIE and typical CIE-active molecule. From mechanistic studies, it is proposed that intramolecular bending should proceed in the excited state, followed by rapid excitation decay. In other words, the “flexible” molecular skeleton is the origin of the deactivation of excitation energy and subsequent emission annihilation through non-radiative decay processes [38]. From this fact, we presume that intrinsic local distortion in the conjugated ligand, which can be readily generated by boron complexation, could be the driving force for presenting emission annihilation in solution through molecular bending activated in the excited state and the key factor in exhibiting solid-state emission by disturbing intermolecular interactions by skeletal distortion. To evaluate the validity of this speculation, a comparison study with potentially distorted and planar molecules is needed.

Herein, we report opposite changes in emission efficiencies between the solution and solid of the modified azomethine–boron complexes **BPhQ** and **BPhQm** with or without skeletal distortion around the boron complexation moiety, respectively. In general, quinoline-based boron complexes have been considered to be a class of highly efficient luminescent dyes in solution owing to their rigid and planar structures [41–44]. Indeed, **BPhQm** possesses a planar structure, while **BPhQ** intrinsically involves distortion, although electronic conjugation can be developed through both molecules. Interestingly, increases and decreases in emission efficiencies by aggregation and crystallization were obtained from **BPhQ** and **BPhQm**, meaning that **BPhQm** shows ACQ in solid, whereas **BPhQ** is an AIE- and CIE-active molecule. From the series of optical measurements, we propose that skeletal distortion plays a critical role in enhanced emission behaviors in solids as well as emission annihilation in solution. This is the first example, to the best of our knowledge, to offer a new design strategy based on the introduction of distortion with boron complexation for realizing AIE and CIE properties.

2. Materials and Methods

According to Scheme 1, the quinoline-based boron complex **BPhQ** was synthesized from the tridentate quinoline ligand **3** (Figures S1–S6 and Schemes S1–S3, See Supplementary Materials). The skeletal distortion was introduced into the quinoline scaffold by the formation of a five-membered ring with a four-coordinating boron atom. We also synthesized the methylene-inserted quinoline

boron complex **BPhQm** as the planar molecule (Figures S7–S9 and Scheme S4, See Supplementary Materials). In the case of **BPhQm**, the double six-membered ring systems were formed by a boron complexation reaction for releasing distortion. To improve the solubility and inhibit undesired aggregation in the solution, **BPhQ** and **BPhQm** were modified with tert-butyl groups. Indeed, the synthesized complexes have good solubility in common organic solvents such as chloroform, THF, and dichloromethane. The structures of **BPhQ** and **BPhQm** were confirmed by ^1H , ^{11}B , ^{13}C NMR, ionization mass measurements and elemental analyses. Fortunately, we obtained single crystals of the complexes suitable for X-ray analyses.



Scheme 1. Synthetic routes of **BPhQ** and **BPhQm**.

3. Results and Discussion

3.1. Single Crystal X-ray Diffraction Analysis

From the comparison with the single-crystal X-ray diffraction (SCXRD) data (Figure 1 and Tables S1–S2, See Supplementary Materials), it was shown that **BPhQ** had a relatively distorted conformation according to the dihedral angle between the quinoline and the adjacent phenyl ring, which was 154.7° . The skeletal distorted conformation should originate from the tightly fused structure involving five- and six-membered rings. In contrast, it was observed that **BPhQm** has a relatively planar structure (the dihedral angle = 168.8°), owing to the loosely fused six-membered ring of the methylene group. From these data, it is evident that both complexes have expected structural features.

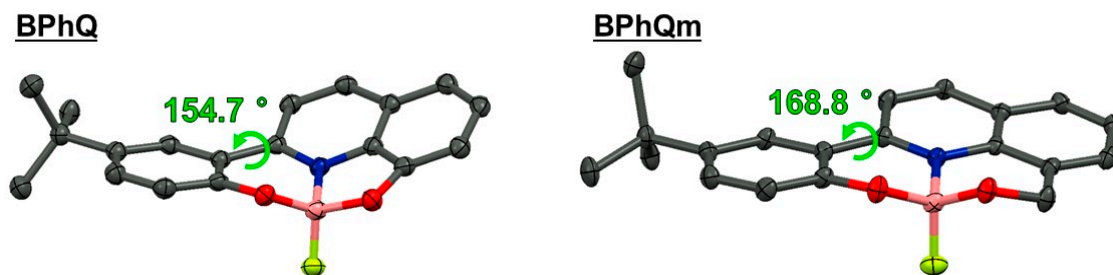


Figure 1. Thermal ellipsoid (probability level 50%) of **BPhQ** (left) and **BPhQm** (right) (gray, carbon atoms; blue, nitrogen atoms; red, oxygen atoms; pink, boron atoms; yellow, fluorine atoms. Hydrogen atoms are omitted for clarity).

3.2. Optical Properties

To evaluate the electronic structures of the complexes in the ground state, the UV–vis absorption spectra were measured with the dilute chloroform solutions (Table 1 and Figure 2a). Similar spectral shapes and molar extinction coefficients were obtained from the absorption bands around 380 nm, indicating that both complexes should have similar electronic structures. It should be noted that the skeletal distortion in **BPhQ** slightly affects the electronic conjugation in the ground state.

Table 1. Optical properties of the synthesized compounds.

Compound	$\lambda_{\text{max,abs}}$ (nm) ^a	ϵ ($10^5 \text{M}^{-1} \text{cm}^{-1}$) ^b	λ_{em} (nm) ^c				Φ_{F} ^d			
			Sol. ^a	Agg. ^e	Film ^f	Cryst. ^g	Sol. ^a	Agg. ^e	Film ^f	Cryst. ^g
BPhQ	377	0.11	550	537	531	518	0.008	0.014	0.021	0.017
BPhQm	387	0.097	493	460	487	479	0.21	0.072	0.16	0.051

^a The longest absorption maximum in 1.0×10^{-5} M chloroform solution. ^b Molar extinction coefficients of the longest absorption band in 1.0×10^{-5} M chloroform solution. ^c Fluorescence maxima with the excitation at the longest absorption maximum. ^d Absolute quantum efficiencies. ^e Prepared from THF/H₂O solutions with a water fraction of 99%. ^f Spin-coated film on the quartz substrate (1 cm \times 5 cm) prepared from chloroform solution (0.10 mL, 1000 rpm). ^g Prepared by the vapor diffusion method (**BPhQ**: from CH₂Cl₂ solution under hexane atmosphere; **BPhQm**: from toluene solution under hexane atmosphere).

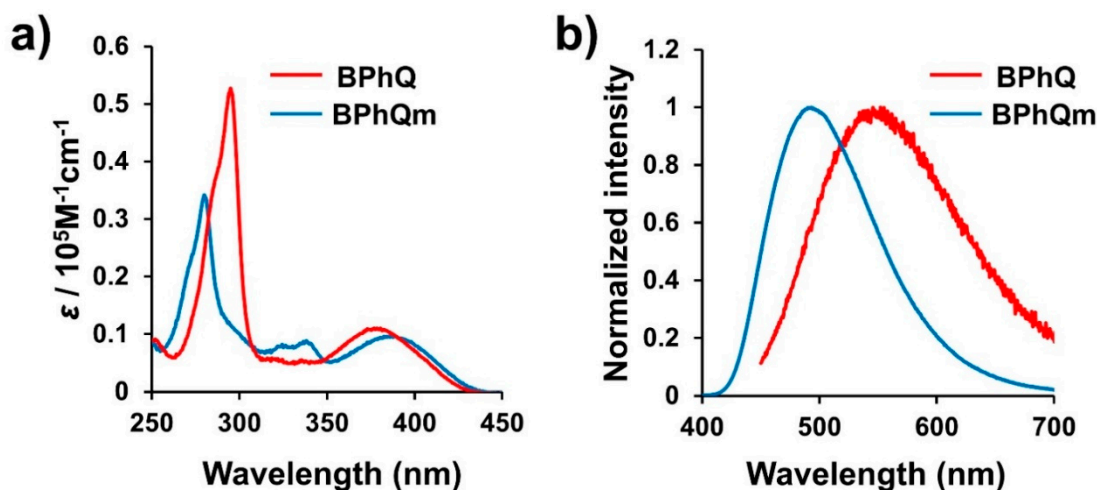


Figure 2. (a) UV–vis absorption and (b) photoluminescence spectra of **BPhQ** and **BPhQm** (1.0×10^{-5} M chloroform solution).

In contrast to the absorption properties, the emission behaviors, representing electronic structures in the excited state, were largely different between both complexes (Figure 2b). We evaluated the photoluminescence (PL) properties of **BPhQ** and **BPhQm** with the same chloroform solutions. The emission band of **BPhQ** was detected in the remarkable red-shifted wavelength region compared

to that of **BPhQm** (**BPhQ**: $\lambda_{em} = 550$ nm; **BPhQm**: $\lambda_{em} = 493$ nm). In particular, a wider Stokes shift was observed from **BPhQ** than from **BPhQm**, meaning that a larger degree of structural relaxation should proceed in **BPhQ** after photo-excitation.

To elucidate the difference in emission wavelength between **BPhQ** and **BPhQm**, a solvatochromism study was executed (Figures S10–S11, See Supplementary Materials). Accordingly, significant shifts in the absorption bands were hardly observed by altering the solvent polarity, whereas the emission bands were bathochromically shifted from 542 to 567 nm for **BPhQ** and from 478 to 512 nm for **BPhQm** as the solvent polarity increased. These results suggest that the emission bands of both boron complexes should be derived from the intramolecular charge transfer (ICT) states. Meanwhile, even in cyclohexane, which is a typical non-polar solvent, there were still pronounced differences between the two emission peak wavelengths (**BPhQ**: $\lambda_{em} = 542$ nm; **BPhQm**: $\lambda_{em} = 478$ nm). In order to obtain deep insight into the origin of the longer-wavelength emission of **BPhQ**, the emissive properties were examined with polystyrene films, including 1 wt% of **BPhQ** or **BPhQm**, where molecular motion would be suppressed in each isolated molecule (Table 2 and Figure S12, See Supplementary Materials). The PL spectrum of the film of **BPhQ** showed an emission band with a clear blue shift from that of the solution ($\lambda_{em,sol.} = 550$ nm, $\lambda_{em,film.} = 531$ nm). In general, the blue-shifted emission in solids is caused by suppressing geometry relaxation in the excited state under a spatially restricted environment compared to the solution [45]. Thus, it is suggested that the longer-wavelength emission of **BPhQ** than that of **BPhQm** should originate from the intrinsic larger degree of molecular mobility in the excited state. Correspondingly, in the PL spectra of **BPhQm** in the polystyrene film, the degree of blue-shift from the solution state was much smaller than that observed in **BPhQ**.

Table 2. Fluorescence lifetime and radiative and non-radiative rate constants of the synthesized compounds.

Compound	τ (ns) ^a				k_r ($\times 10^8 s^{-1}$) ^b				k_{nr} ($\times 10^8 s^{-1}$) ^b			
	Sol. ^c	Agg. ^d	Film ^e	Cryst. ^f	Sol. ^c	Agg. ^d	Film ^e	Cryst. ^f	Sol. ^c	Agg. ^d	Film ^e	Cryst. ^f
BPhQ	0.6	0.3 (4%)	2.1 (32%)	2.0 (66%)	0.12	0.038	0.040	0.065	15	2.7	1.9	3.8
		1.7 (38%)	5.8 (68%)	3.3 (34%)								
		4.3 (58%)										
BPhQm	2.8	1.2 (71%)	0.6 (8%)	0.4 (24%)	0.74	0.26	0.64	0.32	2.8	3.3	3.3	5.9
		3.9 (29%)	1.7 (70%)	1.0 (64%)								
			3.8 (23%)	3.0 (12%)								

^a Emission lifetime at λ_{em} . ^b $k_r = \Phi_F/\tau$, $k_{nr} = (1 - \Phi_F)/\tau$. ^c 1.0×10^{-5} M chloroform solution. ^d Prepared from THF/H₂O solutions with a water fraction of 99%. ^e Spin-coated film on the quartz substrate (1 cm \times 5 cm) prepared from the chloroform solution (0.10 mL, 1000 rpm). ^f Prepared by the vapor diffusion method (**BPhQ**: from CH₂Cl₂ solution under hexane atmosphere; **BPhQm**: from toluene solution under hexane atmosphere).

We evaluated the emission efficiencies of the complexes in the solution, aggregation, and crystalline samples (Table 1 and Figures S13–S14, See Supplementary Materials). From a comparison with the emissive properties in the solution and solid form, it was found that **BPhQ** and **BPhQm** showed opposite behaviors: **BPhQ** had AIE and CIE characteristics, while **BPhQm** showed typical ACQ. We prepared aggregated samples of **BPhQ** and **BPhQm** from THF/H₂O solutions with a water fraction of 99%, and the emission efficiencies were determined as the absolute fluorescence quantum efficiencies (Φ_F). The Φ_F values of the aggregation and crystalline sample for **BPhQ** were significantly higher than those of the solutions ($\Phi_{F,sol.} = 0.008 \rightarrow \Phi_{F,agg.} = 0.014$, $\Phi_{F,cryst.} = 0.017$). On the other hand, the Φ_F values of the aggregated and crystalline sample for **BPhQm** were lower than those of the solution state ($\Phi_{F,sol.} = 0.21 \rightarrow \Phi_{F,agg.} = 0.072$, $\Phi_{F,cryst.} = 0.051$). The reduction in the Φ_F s in the solid of **BPhQm** is likely to be caused by non-specific intermolecular interaction in the condensed state, followed by ACQ.

To examine in detail the photophysical processes especially in **BPhQ**, the radiative (k_r) and non-radiative rate constants (k_{nr})—which represent the sum of the rates in each process with or without emission, respectively—were determined from the lifetime measurements (Table 2 and Figure S15, See Supplementary Materials). Accordingly, it was found that **BPhQ** had a smaller k_r and larger k_{nr} than **BPhQm** in solution, meaning that both the radiative and non-radiative processes should be quite different between **BPhQ** and **BPhQm**. In addition, the k_{nr} s of **BPhQ** in the aggregated and crystalline samples were lowered from those of the solution state, suggesting that the nonradiative decay channels

related to the intramolecular motion of **BPhQ** in the solution state were efficiently restricted under rigid environments, such as in the aggregation and crystal. A similar enhancement of Φ_F was also observed in 1 wt% polystyrene dispersed film (Table 2 and Figure S15, See Supplementary Materials). The Φ_F of **BPhQ** in the polystyrene film was determined as 0.021, which is higher than that of the solution state ($\Phi_F = 0.008$), whereas it was found that the k_{nr} in the polystyrene film was one order lower than that in the solution state, representing that the improvement of the emission property in film should be associated with the restriction of molecular motions by polymer chains. Contrary to **BPhQ**, the Φ_F of **BPhQm** decreased in the polystyrene film compared with that in the solution, and both of the k_{nr} values were in the same range, suggesting that the molecular motions of **BPhQm** in the excited state hardly play a role in the emission properties of the solution state because of its rigid molecular structure. In summary, from the comparison with both complexes, it was figured out that **BPhQ** had a larger non-radiative rate constant. Possibly, the distorted structure in **BPhQ** induced by boron complexation may cause geometrical perturbation in the excited state, and thus the molecular motions promoted non-radiative decay processes.

3.3. Packing Structures

To comprehend the solid-state luminescent properties, we compared the molecular packing structures of the complexes determined by the SCXRD data (Figure 3). Although both complexes belong to the triclinic system (*P1* space group), the packing structures were different, probably because of the planarity of **BPhQ** and **BPhQm**. In the crystalline packing of **BPhQ**, each molecule formed π - π intermolecular interactions between dimers, with distance of 3.596 Å. However, in another molecular surface, the distance to the adjacent molecule was 4.148 Å, and thus the π - π intermolecular interactions through three or more molecules were inhibited, owing to the steric hindrance imposed by the distorted π -conjugated system and the protruded fluorine atom. In contrast, the molecules of **BPhQm** with a planar structure were densely packed into molecular columns that were perpendicular to the quinoline moieties and formed face-to-face π - π interactions between both surfaces, with distances of 3.723 and 3.807 Å. From these structural data, it is proposed that π - π interactions through multiple **BPhQ** molecules can be disturbed owing to the distorted structure, followed by avoiding ACQ. On the other hand, because of the intrinsic planar structure of **BPhQm**, a critical ACQ should be induced through tight intermolecular interactions, such as π - π stacking, in the solid state.

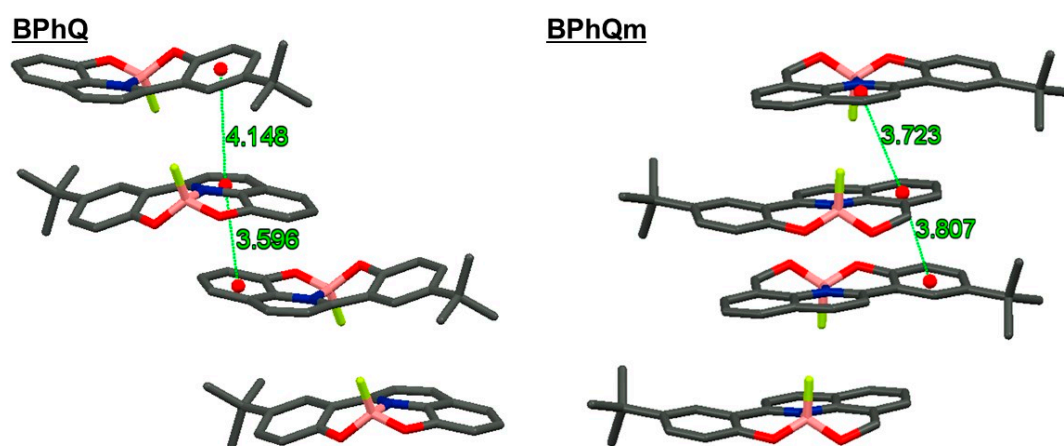


Figure 3. Packing structures of **BPhQ** (left) and **BPhQm** (right) (gray, carbon atoms; blue, nitrogen atoms; red, oxygen atoms; pink, boron atoms; yellow, fluorine atoms. Hydrogen atoms are omitted for clarity).

3.4. Theoretical Calculation

In order to support the emissive properties and radiative decay processes of **BPhQ** and **BPhQm**, we conducted time-dependent density functional theory (TD-DFT) calculations at the B3LYP/6-311 + G(d,p)

level with the optimized structures in the S_1 states (Table 3). Figure 4 represents highest occupied molecular orbitals (HOMOs) and lowest unoccupied molecular orbitals (LUMOs) at the S_1 state. The LUMOs of both molecules are delocalized on the entire molecules, while the HOMOs are localized on the quinoline moiety and the tert-butyl group-substituted phenyl ring, respectively. These alterations in the electronic orbital distributions between HOMO and LUMO correspond to the ICT characters of the emission bands of both complexes. The electron-rich oxygen atom might contribute to the localization of HOMO of **BPhQ** at the quinolone moiety, while the electron donation by the quinoline moiety might be weak in **BPhQm**, and subsequently HOMO might be able to spread in the tert-butyl group-substituted phenyl ring.

Table 3. Photophysical parameters obtained by TD-DFT/B3LYP/6-311 + G(d,p) based on the optimized geometries in the S_1 state.

Compound	Excitation Energy	$S_1 \rightarrow S_0$ Transition Contribution	Oscillator Strength	μ^a
BPhQ	2.30 eV (540 nm)	HOMO–LUMO (94%)	0.0262	0.4656 a.u.
BPhQm	2.57 eV (482 nm)	HOMO–LUMO (95%)	0.1521	2.415 a.u.

^a Transition dipole moment.

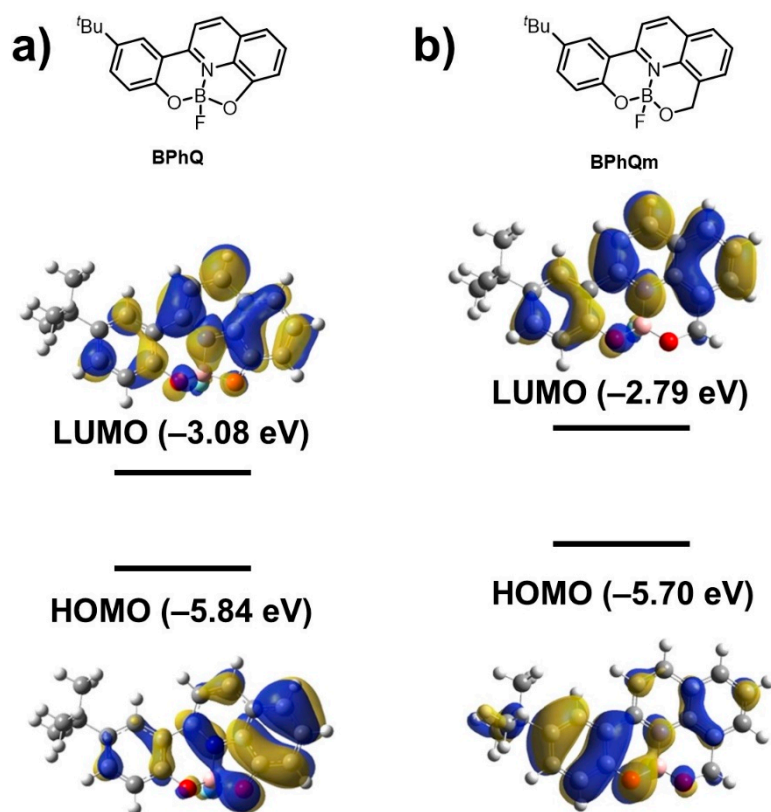


Figure 4. Structures and molecular orbital diagrams for the lowest unoccupied molecular orbital (LUMO) and highest occupied molecular orbital (HOMO) of (a) **BPhQ** (b) **BPhQm** calculated at B3LYP/6-311 + G(d,p) with S_1 state optimized structures.

Finally, we examined the electronic transitions with theoretical calculations. The oscillator strength (f) for the S_1 to S_0 transition, which is associated with k_r , was quite small ($f = 0.0262$) in **BPhQ**, proposing that the lowest-lying excited state S_1 should be a weak emissive state. In contrast, the f value of **BPhQm** was about six times higher than that of **BPhQ** ($f = 0.1521$)—that is, the lowest-lying excited state S_1 is a highly emissive state. These theoretical results were in good agreement with the

experimental k_r data (Tables 2 and 3). Additionally, to reveal the origin of the difference in the oscillator strength for the $S_1 \rightarrow S_0$ transition between **BPhQ** and **BPhQm**, the transition densities (ρ) for the corresponding transitions were calculated for a simple and effective representation of the electronic transition (Figure 5). The magnitude of the f for an electronic transition is proportional to the square of the transition dipole moment (μ). On the other hand, μ can be expressed by the following equation:

$$\mu = \int \rho(x)(-ex)dx \quad (1)$$

where ρ is the transition density for the S_1 state and x denotes a point in three-dimensional space. From the equation, the μ value becomes large when ρ has a value at x at which these elements are large—i.e., when ρ is distributed in the regions that are distant from the coordinate origin [46,47]. Figure 5 shows a more widely distributed ρ in **BPhQm**, indicating that the overlap between the HOMO and LUMO was larger than that in **BPhQ**. Owing to this wide ρ distribution spread to the entire molecule, **BPhQm** has moderate μ of 2.415 (a.u.). In contrast, **BPhQ** has a small μ of 0.4656 (a.u.), since the ρ distribution range is limited in the small regions around the quinoline moiety. This is because the HOMO of **BPhQ** is mainly distributed in the quinoline group (Figure 4), and the resulting HOMO–LUMO overlap is thus small. In the presence and absence of the methylene group, the electronic structures are also influenced.

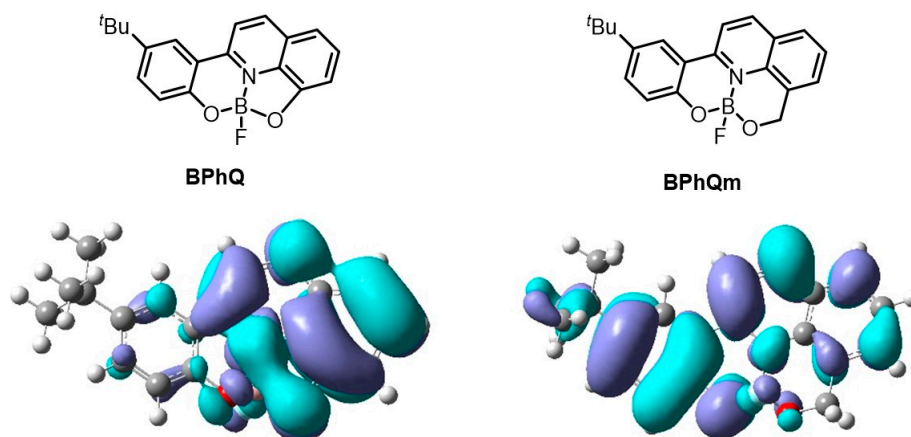


Figure 5. Transition densities ρ associated with the $S_1 \rightarrow S_0$ excitation of (a) **BPhQ** and (b) **BPhQm**. The isosurface value for ρ is 0.0004 atomic units (purple regions: positive; blue regions: negative).

4. Conclusions

We demonstrate that the introduction of skeletal distortion by boron complexation with the tridentate ligand is a facile strategy for obtaining AIE and CIE-active molecules. From the comparison with phenyl quinoline-based boron complexes **BPhQ** and **BPhQm** with or without critical skeletal distortion around the boron complex moiety, it was found that with the molecular motions, represented by the wider Stokes shift, a smaller k_r and larger k_{nr} are feasible in the excited state, followed by emission annihilation, even though electronic conjugation can be developed through planar molecular structures in the ground state. Further, molecular distortion seems to play a positive role in avoiding ACQ. Consequently, we observed from both complexes contrary changes in emission efficiencies by aggregation, such as AIE and CIE from **BPhQ** and ACQ from **BPhQm**. So far, boron complexation has been applied for constructing a robust conjugated system, while we herein present a new manner of boron complexation through the generation of distortion for a potential movable point in the excited state as well as for realizing emission enhancement in the solid state. Thus, it is implied that conjugated element-blocks with distortion might be a promising platform for obtaining advanced stimuli-responsive optical materials.

Supplementary Materials: Supplementary materials are available online at <http://www.mdpi.com/2073-4352/10/7/615/s1>. Scheme S1: Synthesis of compound 1. Figure S1: ^1H NMR spectrum of 1, CDCl_3 , 400 MHz. Scheme S2: Synthesis of compound 2. Figure S2: ^1H NMR spectrum of 2, CDCl_3 , 400 MHz. Figure S3: ^{13}C NMR spectrum of 2, CDCl_3 , 100 MHz. Scheme S3: Synthesis of BPhQ. Figure S4: ^1H NMR spectrum of BPhQ, CDCl_3 , 400 MHz. Figure S5: ^{11}B NMR spectrum of BPhQ, CDCl_3 , 128 MHz. Figure S6: ^{13}C NMR spectrum of BPhQ, CDCl_3 , 100 MHz. Scheme S4: Synthesis of BPhQm. Figure S7: ^1H NMR spectrum of BPhQm, CDCl_3 , 400 MHz. Figure S8: ^{11}B NMR spectrum of BPhQm, CDCl_3 , 128 MHz. Figure S9: ^{13}C NMR spectrum of BPhQm, CDCl_3 , 100 MHz. Table S1: Crystallographic data of BPhQ at 93 K. Table S2: Crystallographic data of BPhQm at 93 K. Figure S10: UV-vis absorption (left) and PL spectra (right) of BPhQ in the diluted solutions (1.0×10^{-5} M) at room temperature. Figure S11: UV-vis absorption (left) and PL spectra (right) of BPhQm in the diluted solutions (1.0×10^{-5} M) at room temperature. Figure S12: PL spectra of BPhQ and BPhQm in the 1 wt% polystyrene dispersed films. Figure S13: PL spectra of BPhQ and BPhQm in aggregated states ($\text{THF}/\text{H}_2\text{O} = 1/99$, 1.0×10^{-4} M). Figure S14: PL spectra of BPhQ and BPhQm in crystalline states. Figure S15: PL lifetime decay curves of BPhQ and BPhQm in chloroform solution (1.0×10^{-5} M), 1 wt% polystyrene film, the aggregated and crystalline states at room temperature. Their emissions at the PL peak tops were monitored.

Author Contributions: Conceptualization, S.O.; data curation, S.O.; funding acquisition, M.G., K.T., and Y.C.; investigation, S.O.; project administration, K.T.; supervision, K.T.; writing—original draft, S.O.; writing—review and editing, M.G., K.T., and Y.C. All authors have read and agreed to the published version of the manuscript.

Funding: This research received no external funding.

Acknowledgments: This work was partially supported by a Kyoto University Foundation (for M.G.), a Grant-in-Aid for Young Scientists (for M.G.) (JSPS KAKENHI Grant numbers 20K15334), Grant-in-Aid for Scientific Research (B) (JSPS KAKENHI Grant numbers 17H03067) and (A) (JSPS KAKENHI Grant numbers 17H01220), Grant-in-Aid for Scientific Research on Innovative Areas “New Polymeric Materials Based on Element-Blocks (No.2401)” (JSPS KAKENHI Grant Number 24102013) and Challenging Research (Pioneering) (JSPS KAKENHI Grant Number 18H05356).

Conflicts of Interest: The authors declare no conflict of interest.

References

1. Yuan, L.; Lin, W.; Zheng, K.; He, L.; Huang, W. Far-red to near infrared analyte-responsive fluorescent probes based on organic fluorophore platforms for fluorescence imaging. *Chem. Soc. Rev.* **2013**, *42*, 622–661. [[CrossRef](#)] [[PubMed](#)]
2. Zheng, M.; Tan, H.; Xie, Z.; Zhang, L.; Jing, X.; Sun, Z. Fast Response and High Sensitivity Europium Metal Organic Framework Fluorescent Probe with Chelating Terpyridine Sites for Fe^{3+} . *ACS Appl. Mater. Interfaces* **2013**, *5*, 1078–1083. [[CrossRef](#)] [[PubMed](#)]
3. Gonçalves, M.S.T. Fluorescent Labeling of Biomolecules with Organic Probes. *Chem. Rev.* **2009**, *109*, 190–212. [[CrossRef](#)]
4. Thompson, B.C.; Madrigal, L.G.; Pinto, M.R.; Kang, T.; Schanze, K.S.; Reynolds, J.R. Donor–acceptor copolymers for red-and near-infrared-emitting polymer light-emitting diodes. *J. Polym. Sci. Part A Polym. Chem.* **2005**, *43*, 1417–1431. [[CrossRef](#)]
5. Dias, F.B.; Bourdakos, K.N.; Jankus, V.; Moss, K.C.; Kamtekar, K.T.; Bhalla, V.; Santos, J.; Bryce, M.R.; Monkman, A.P. Triplet Harvesting with 100% Efficiency by Way of Thermally Activated Delayed Fluorescence in Charge Transfer OLED Emitters. *Adv. Mater.* **2013**, *25*, 3707–3714. [[CrossRef](#)] [[PubMed](#)]
6. Wong, W.-Y.; Ho, C.-L. Functional metallophosphors for effective charge carrier injection/transport: New robust OLED materials with emerging applications. *J. Mater. Chem.* **2009**, *19*, 4457–4482. [[CrossRef](#)]
7. Ding, L.; Dong, S.-C.; Jiang, Z.-Q.; Chen, H.; Liao, L.-S. Orthogonal Molecular Structure for Better Host Material in Blue Phosphorescence and Larger OLED White Lighting Panel. *Adv. Funct. Mater.* **2015**, *25*, 645–650. [[CrossRef](#)]
8. Chujo, Y.; Tanaka, K. New Polymeric Materials Based on Element-Blocks. *Bull. Chem. Soc. Jpn.* **2015**, *88*, 633–643. [[CrossRef](#)]
9. Gon, M.; Tanaka, K.; Chujo, Y. Recent progress in the development of advanced element-block materials. *Polym. J.* **2017**, *50*, 109–126. [[CrossRef](#)]
10. Tanaka, K.; Chujo, Y. Modulation of the solid-state luminescent properties of conjugated polymers by changing the connecting points of flexible boron element blocks. *Polym. J.* **2020**, *52*, 555–566. [[CrossRef](#)]

11. Matsumura, Y.; Ishidoshiro, M.; Irie, Y.; Imoto, H.; Naka, K.; Tanaka, K.; Inagi, S.; Tomita, I. Arsole-Containing π -Conjugated Polymer by the Post-Element-Transformation Technique. *Angew. Chem. Int. Ed.* **2016**, *55*, 15040–15043. [[CrossRef](#)] [[PubMed](#)]
12. Wakabayashi, J.; Gon, M.; Tanaka, K.; Chujo, Y. A Near-Infrared Absorptive and Emissive Poly(*p*-phenylene vinylene) Derivative Containing Azobenzene–Boron Complexes. *Macromolecules* **2020**, *53*, 4524–4532. [[CrossRef](#)]
13. Ohtani, S.; Nakamura, M.; Gon, M.; Tanaka, K.; Chujo, Y. Synthesis of Fully-Fused Bisboron Azomethine Complexes and Their Conjugated Polymers with Solid-State Near-Infrared Emission. *Chem. Commun.* **2020**, *56*, 6575–6578. [[CrossRef](#)] [[PubMed](#)]
14. Gon, M.; Wakabayashi, J.; Tanaka, K.; Chujo, Y. Unique Substitution Effect at 5,5'-Positions of Fused Azobenzene–Boron Complexes with a N=N π -Conjugated System. *Chem. Asian J.* **2019**, *14*, 1837–1843. [[CrossRef](#)] [[PubMed](#)]
15. Ohtani, S.; Gon, M.; Tanaka, K.; Chujo, Y. Construction of the Luminescent Donor–Acceptor Conjugated Systems Based on Boron-Fused Azomethine Acceptor. *Macromolecules* **2019**, *52*, 3387–3393. [[CrossRef](#)]
16. Gon, M.; Tanaka, K.; Chujo, Y. A Highly Efficient Near-Infrared-Emissive Copolymer with a N=N Double-Bond π -Conjugated System Based on a Fused Azobenzene–Boron Complex. *Angew. Chem. Int. Ed.* **2018**, *57*, 6546–6551. [[CrossRef](#)]
17. Loudet, A.; Burgess, K. BODIPY Dyes and Their Derivatives: Syntheses and Spectroscopic Properties. *Chem. Rev.* **2007**, *107*, 4891–4932. [[CrossRef](#)]
18. Ulrich, G.; Zissel, R.; Harriman, A. The Chemistry of Fluorescent Bodipy Dyes: Versatility Unsurpassed. *Angew. Chem. Int. Ed.* **2008**, *47*, 1184–1201. [[CrossRef](#)]
19. Frath, D.; Azizi, S.; Ulrich, G.; Retailleau, P.; Zissel, R. Facile Synthesis of Highly Fluorescent Boranil Complexes. *Org. Lett.* **2011**, *13*, 3414–3417. [[CrossRef](#)]
20. Frath, D.; Massue, J.; Ulrich, G.; Zissel, R. Luminescent Materials: Locking π -Conjugated and Heterocyclic Ligands with Boron(III). *Angew. Chem. Int. Ed.* **2014**, *53*, 2290–2310. [[CrossRef](#)]
21. Suresh, D.; Ferreira, B.; Lopes, P.S.; Gomes, C.S.B.; Krishnamoorthy, P.; Charas, A.; Vila-Viçosa, D.; Morgado, J.; Calhorda, M.J.; Maçanita, A.L.; et al. Boron complexes of aromatic ring fused iminopyrrolyl ligands: Synthesis, structure, and luminescence properties. *Dalton Trans.* **2016**, *45*, 15603–15620. [[CrossRef](#)] [[PubMed](#)]
22. Zhang, G.; Chen, J.; Payne, S.J.; Kooi, S.E.; Demas, J.N.; Fraser, C.L. Multi-Emissive Difluoroboron Dibenzoylmethane Polylactide Exhibiting Intense Fluorescence and Oxygen-Sensitive Room-Temperature Phosphorescence. *J. Am. Chem. Soc.* **2007**, *129*, 8942–8943. [[CrossRef](#)] [[PubMed](#)]
23. Hesari, M.; Barbon, S.M.; Staroverov, V.N.; Ding, Z.; Gilroy, J.B. Efficient electrochemiluminescence of a readily accessible boron difluoride formazanate dye. *Chem. Commun.* **2015**, *51*, 3766–3769. [[CrossRef](#)] [[PubMed](#)]
24. Vuong, T.M.H.; Weimmerskirch-Aubatin, J.; Lohier, J.-F.; Bar, N.; Boudin, S.; Labbé, C.; Gourbilleau, F.; Nguyen, H.; Dang, T.T.; Villemin, D. Blue highly fluorescent boron difluoride complexes based on phthalazine–pyridine. *New J. Chem.* **2016**, *40*, 6070–6076. [[CrossRef](#)]
25. Ando, N.; Soutome, H.; Yamaguchi, S. Near-infrared fluorescein dyes containing a tricoordinate boron atom. *Chem. Sci.* **2019**, *10*, 7816–7821. [[CrossRef](#)]
26. Li, D.; Wang, K.; Huang, S.; Qu, S.; Liu, X.; Zhu, Q.; Zhang, H.; Wang, Y. Brightly fluorescent red organic solids bearing boron-bridged π -conjugated skeletons. *J. Mater. Chem.* **2011**, *21*, 15298–15304. [[CrossRef](#)]
27. Urban, M.; Durka, K.; Górka, P.; Wiosna-Sałyga, G.; Nawara, K.; Jankowski, P.; Luliński, S. The effect of locking π -conjugation in organoboron moieties in the structures of luminescent tetracoordinate boron complexes. *Dalton Trans.* **2019**, *48*, 8642–8663. [[CrossRef](#)]
28. Wakamiya, A.; Taniguchi, T.; Yamaguchi, S. Intramolecular B–N Coordination as a Scaffold for Electron-Transporting Materials: Synthesis and Properties of Boryl-Substituted Thienylthiazoles. *Angew. Chem. Int. Ed.* **2006**, *45*, 3170–3173. [[CrossRef](#)]
29. Yoshino, J.; Kano, N.; Kawashima, T. Synthesis of the most intensely fluorescent azobenzene by utilizing the B–N interaction. *Chem. Commun.* **2007**, 559–561. [[CrossRef](#)]
30. Yoshino, J.; Kano, N.; Kawashima, T. Fluorescence Properties of Simple N-Substituted Aldimines with a B–N Interaction and Their Fluorescence Quenching by a Cyanide Ion. *J. Org. Chem.* **2009**, *74*, 7496–7503. [[CrossRef](#)]

31. Kwok, R.T.K.; Leung, C.W.T.; Lam, J.W.Y.; Tang, B.Z. Biosensing by luminogens with aggregation-induced emission characteristics. *Chem. Soc. Rev.* **2015**, *44*, 4228–4238. [[CrossRef](#)] [[PubMed](#)]
32. Mei, J.; Leung, N.L.C.; Kwok, R.T.K.; Lam, J.W.Y.; Tang, B.Z. Aggregation-Induced Emission: Together We Shine, United We Soar! *Chem. Rev.* **2015**, *115*, 11718–11940. [[CrossRef](#)] [[PubMed](#)]
33. Luo, J.; Xie, Z.; Lam, J.W.Y.; Cheng, L.; Chen, H.; Qiu, C.; Kwok, H.S.; Zhan, X.; Liu, Y.; Zhu, D.; et al. Aggregation-induced emission of 1-methyl-1,2,3,4,5-pentaphenylsilole. *Chem. Commun.* **2001**, 1740–1741. [[CrossRef](#)] [[PubMed](#)]
34. Hong, Y.; Lam, J.W.Y.; Tang, B.Z. Aggregation-induced emission. *Chem. Soc. Rev.* **2011**, *40*, 5361–5388. [[CrossRef](#)]
35. Dong, Y.; Lam, J.W.Y.; Qin, A.; Li, Z.; Sun, J.; Sung, H.H.-Y.; Williams, I.D.; Tang, B.Z. Switching the light emission of (4-biphenyl)phenyldibenzofulvene by morphological modulation: Crystallization-induced emission enhancement. *Chem. Commun.* **2007**, 40–42. [[CrossRef](#)] [[PubMed](#)]
36. Galer, P.; Korošec, R.C.; Vidmar, M.; Šket, B. Crystal Structures and Emission Properties of the BF₂ Complex 1-Phenyl-3-(3,5-dimethoxyphenyl)-propane-1,3-dione: Multiple Chromisms, Aggregation- or Crystallization-Induced Emission, and the Self-Assembly Effect. *J. Am. Chem. Soc.* **2014**, *136*, 7383–7394. [[CrossRef](#)]
37. Yoshii, R.; Hirose, A.; Tanaka, K.; Chujo, Y. Functionalization of Boron Diiminates with Unique Optical Properties: Multicolor Tuning of Crystallization-Induced Emission and Introduction into the Main Chain of Conjugated Polymers. *J. Am. Chem. Soc.* **2014**, *136*, 18131–18139. [[CrossRef](#)]
38. Gon, M.; Tanaka, K.; Chujo, Y. Concept of Excitation-Driven Boron Complexes and Their Applications for Functional Luminescent Materials. *Bull. Chem. Soc. Jpn.* **2019**, *92*, 7–18. [[CrossRef](#)]
39. Tanaka, K.; Nishino, K.; Ito, S.; Yamane, H.; Suenaga, K.; Hashimoto, K.; Chujo, Y. Development of Solid-State Emissive *o*-Carborane and Theoretical Investigation of the Mechanism of the Aggregation-Induced Emission Behaviors of Organoboron “Element-Blocks”. *Faraday Discuss.* **2017**, *196*, 31–42. [[CrossRef](#)]
40. Ohtani, S.; Gon, M.; Tanaka, K.; Chujo, Y. A Flexible, Fused, Azomethine–Boron Complex: Thermochromic Luminescence and Thermosensitive Behavior in Structural Transitions between Crystalline Polymorphs. *Chem. Eur. J.* **2017**, *23*, 11827–11833. [[CrossRef](#)]
41. Ma, R.-Z.; Yao, Q.-C.; Yang, X.; Xia, M. Synthesis, characterization and photoluminescence properties of strong fluorescent BF₂ complexes bearing (2-quinolin-2-yl) phenol ligands. *J. Fluorine Chem.* **2012**, *137*, 93–98. [[CrossRef](#)]
42. Tokoro, Y.; Nagai, A.; Kokado, K.; Chujo, Y. Synthesis of Organoboron Quinoline-8-thiolate and Quinoline-8-selenolate Complexes and Their Incorporation into the π -Conjugated Polymer Main-Chain. *Macromolecules* **2009**, *42*, 2988–2993. [[CrossRef](#)]
43. Balijapalli, U.; Iyer, S.K. Synthesis and Optical Properties of a Series of Green-Light-Emitting 2-(4-Phenylquinolin-2-yl)phenol–BF₂ Complexes (Boroquinols). *Eur. J. Org. Chem.* **2015**, *2015*, 5089–5098. [[CrossRef](#)]
44. Qi, Y.; Kang, R.; Huang, J.; Zhang, W.; He, G.; Yin, S.; Fang, Y. Reunderstanding the Fluorescent Behavior of Four-Coordinate Monoboron Complexes Containing Monoanionic Bidentate Ligands. *J. Phys. Chem. B* **2017**, *121*, 6189–6199. [[CrossRef](#)]
45. Shi, J.; Aguilar Suarez, L.E.; Yoon, S.-J.; Varghese, S.; Serpa, C.; Park, S.Y.; Lüer, L.; Roca-Sanjuán, D.; Milián-Medina, B.; Gierschner, J. Solid State Luminescence Enhancement in π -Conjugated Materials: Unraveling the Mechanism beyond the Framework of AIE/AIEE. *J. Phys. Chem. C* **2017**, *121*, 23166–23183. [[CrossRef](#)]
46. Ma, L.; Yu, Y.; Jiao, B.; Hou, X.; Wu, Z. Theoretical evidence of low-threshold amplified spontaneous emission in organic emitters: Transition density and intramolecular vibrational mode analysis. *Phys. Chem. Chem. Phys.* **2018**, *20*, 19515–19524. [[CrossRef](#)]
47. Shizu, K.; Noda, H.; Tanaka, H.; Taneda, M.; Uejima, M.; Sato, T.; Tanaka, K.; Kaji, H.; Adachi, C. Highly Efficient Blue Electroluminescence Using Delayed-Fluorescence Emitters with Large Overlap Density between Luminescent and Ground States. *J. Phys. Chem. C* **2015**, *119*, 26283–26289. [[CrossRef](#)]

